

A Universal Degradation-based Bridging Technique for Domain Adaptive Semantic Segmentation

Wangkai Li¹, Rui Sun¹, Tianzhu Zhang^{1*}

¹School of Information Science and Technology, University of Science and Technology of China, Hefei, 230027, China.

*Corresponding author(s). E-mail(s): tzzhang@ustc.edu.cn;
Contributing authors: lwklwk@mail.ustc.edu.cn; issunrui@mail.ustc.edu.cn;

Abstract

Semantic segmentation often suffers from significant performance degradation when the trained network is applied to a different domain. To address this issue, unsupervised domain adaptation (UDA) has been extensively studied. Existing methods introduce the domain bridging techniques to mitigate substantial domain gap, which construct intermediate domains to facilitate the gradual transfer of knowledge across different domains. However, these strategies often require dataset-specific designs and may generate unnatural intermediate distributions that lead to semantic shift. In this paper, we propose DiDA, a universal degradation-based bridging technique formalized as a diffusion forward process. DiDA consists of two key modules: (1) Degradation-based Intermediate Domain Construction, which creates continuous intermediate domains through simple image degradation operations to encourage learning domain-invariant features as domain differences gradually diminish; (2) Semantic Shift Compensation, which leverages a diffusion encoder to encode and compensate for semantic shift information with degraded time-steps, preserving discriminative representations in the intermediate domains. As a plug-and-play solution, DiDA supports various degradation operations and seamlessly integrates with existing UDA methods. Extensive experiments on prevalent synthetic-to-real semantic segmentation benchmarks demonstrate that DiDA consistently improves performance across different settings and achieves new state-of-the-art results when combined with existing methods.

Keywords: Unsupervised domain adaptation, semantic segmentation, domain bridging

1 Introduction

Semantic segmentation, a fine-grained pixel-wise classification task, assigns semantic class labels to each pixel, facilitating high-level image analysis. Despite the remarkable progress made in this field (Long et al., 2015; Chen et al., 2017; Cheng et al., 2021, 2022), networks trained within source domain often encounter significant performance degradation when applied to a target dataset due to domain discrepancies. Mitigating this issue to

enhance the generalization capability of networks remains a formidable challenge. To address this problem, extensive research has resorted to unsupervised domain adaptation (UDA), which aims to transfer knowledge from a labeled source domain to an unlabeled target domain.

In previous works, domain bridging techniques have been introduced to mitigate the substantial differences between target and source domains. These techniques construct intermediate domains

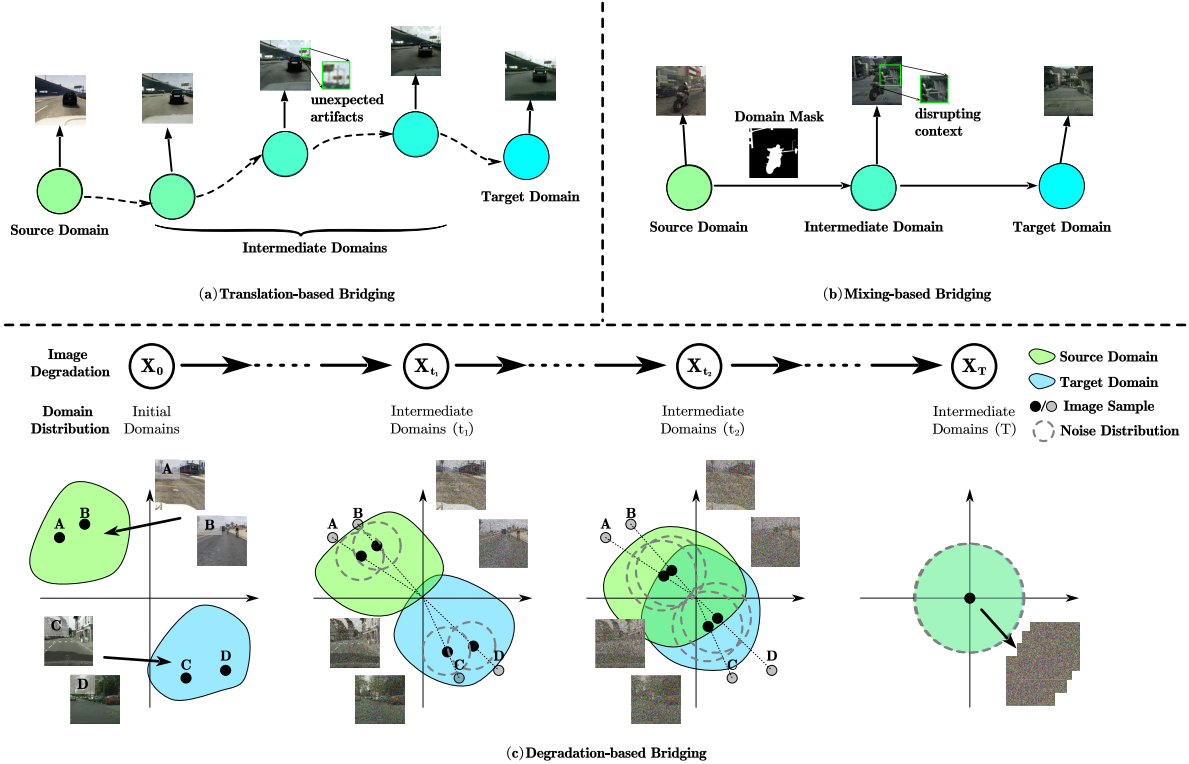


Fig. 1 Comparison of domain bridging techniques for generating intermediate distributions. (a) Translation-based methods transfer the style of source data to target data but may generate artifacts. (b) Mixing-based methods blend images from different domains but may disrupt contextual information. (c) Our degradation-based approach constructs dataset-agnostic intermediate domains and formalizes them as a diffusion forward process while alleviating semantic shift by associating shift information with degraded time-steps, providing a more generalized and effective solution.

in the input space to facilitate the gradual transfer of knowledge across different domains, which can be categorized into two paradigms. The first paradigm focuses on image translation (Murez et al., 2018; Hoffman et al., 2018; Zhu et al., 2017) to transfer the style of source data to target data (see Fig. 1(a)). Some methods in this paradigm (Gong et al., 2019; Peng et al., 2023) control the degree of style transfer to obtain a sequence of intermediate domains shifting from source domain to target domain, thereby bridging the distribution gap between two domains. Although intuitive, these approaches require extra training costs for translation networks and are prone to generating unexpected artifacts without preserving the original semantic information, leading to sub-optimal adaptation performance. The second paradigm utilizes image mixing-based data augmentation methods (Tranheden et al., 2021; Olsson et al., 2021; Zhou et al., 2022) to blend images from different domains (see Fig. 1(b)). While this

paradigm can effectively construct intermediate domain distributions and exhibit strong performance improvements, such as unnatural stitching strategies may compromise contextual information and result in semantic confusion (Chen et al., 2022). To ensure effective adaptation, it is crucial to carefully design a blending strategy (Yang and Soatto, 2020; Olsson et al., 2021) and determine the appropriate mixing ratios (Huo et al., 2023; Chen et al., 2022), which are often designed manually based on prior knowledge of specific dataset characteristics.

Based on the above discussion, we observe that the core idea of domain bridging techniques can be summarized as establishing intermediate distribution between source domain distribution and target domain distribution, gradually enhancing the network’s cross-domain adaptation ability by learning domain-shared features from these intermediate distributions. However, existing approaches face two critical challenges. (1)

Their application requires either additional translation network training or careful design of domain mixing strategies specific to the dataset, making these strategies lacking flexibility and reliant on *dataset-specific* prior knowledge. (2) Whether based on translation or mixing methods, the constructed intermediate domains result in unnatural image distribution, i.e., deviating from the real image distribution, caused by generating unexpected artifacts (translation-based methods) or disrupting contextual information (mixing-based methods). This hinders the network from learning discriminative representations, a problem known as semantic shift (Bai et al., 2022; Wang et al., 2021). Semantic shift refers to the phenomenon where aggressive perturbation of the image distribution causes a misalignment between the perturbed images and their corresponding semantic labels. How to model the semantic shift existing in intermediate domain is still *intractable* and under-explored.

These challenges motivate us to explore a concise and universal approach to directly construct intermediate data distributions while addressing semantic shift. We find an interesting fact that simple image degradation operations, which apply the same degree of disturbances to images from different domains, can be seen as a domain bridging mechanism. To illustrate this phenomenon, we define a series of intermediate distributions between the real data distributions (source or target) and an elementary (Gaussian) distribution with the aid of a forward diffusion process (Ho et al., 2020) by gradually adding noise (see Fig. 1(c)). During this process, the distribution discrepancy between the two domains gradually decreases, and different samples eventually collapse into the same distribution. This construction approach has a two-fold benefit: (1) It implies that we can use simple image degradation operations to obtain intermediate domain images and enhance the network’s adaptation ability. This direct construction of intermediate distributions is *dataset-agnostic* and exhibits strong flexibility to implement, which can be seen as a universal bridging technique; (2) Since we explicitly define continuous intermediate domain distributions through a Markov chain, the shifted semantic information in the intermediate domains can be associated with corresponding degraded time-steps. This makes the semantic shift issue *solvable* by leveraging the

encoded degradation time-step prior, allowing us to compensate for the discriminative representations lost due to semantic shift.

In this paper, we propose a degradation-based bridging approach, namely DiDA, which constructs intermediate domains through simple dataset-agnostic image degradation operations, and formalizes them as a **D**iffusion forward process while alleviating semantic shift caused by unnatural image distribution, for **D**omain **A**daptive semantic segmentation. We make the following designs to couple diffusion strategies with the UDA training pipeline, including two key modules: Degradation-based Intermediate Domain Construction and Semantic Shift Compensation. (1) In Degradation-based Intermediate Domain Construction module, we introduce a universal technique that creates continuous intermediate domains using simple degradation operations. By formalizing this process as a diffusion forward process and integrating it into UDA training, we encourage the network to learn domain-invariant features as domain differences progressively diminish. (2) In Semantic Shift Compensation module, we leverage a diffusion encoder to capture semantic shift information associated with degradation time-steps. Through residual connections between hierarchical features, we compensate for lost discriminative representations in intermediate domains, ensuring better alignment between features and semantic labels. (3) To further validate the effectiveness of above two modules, we employ multiple different degradation operations to construct our method, demonstrating the flexibility and expansibility of DiDA. The implementation of DiDA can be built with any other choice of image degradation by replacing the operation of adding Gaussian noise in a standard diffusion setting. This showcases the versatility of our approach and its potential to be adapted to various degradation techniques. Note that our method can be seen as a plug-and-play bridging technique that can be built with multiple UDA methods and network architectures, consistently showing performance improvements.

In this work, our contributions can be summarized as follows:

- (1) We propose a plug-and-play, dataset-agnostic domain bridging mechanism based on universal degradation operations, addressing the

limitations of previous methods that rely on dataset-specific prior knowledge.

- (2) We formalize our bridging technique as a diffusion forward process, employing continuous degradation operations to gradually reduce distribution discrepancy between domains, and integrate it into UDA training.
- (3) We design a novel framework that couples diffusion strategies with UDA training to effectively alleviate semantic shift in intermediate domains through explicit temporal modeling.
- (4) Extensive experiments on two standard UDA semantic segmentation benchmarks demonstrate the effectiveness of our approach. When combined with existing methods, DiDA consistently improves their performance and achieves new state-of-the-art results.

2 Related Work

2.1 Unsupervised Domain Adaptation (UDA)

Unsupervised Domain Adaptation (UDA) aims to transfer the knowledge of semantics learned from labeled source domains to unlabeled target domains. Due to the ubiquity of domain gaps, UDA methods have been widely studied for various computer vision fields, including image classification (Ghifary et al., 2016; Ganin et al., 2016; Long et al., 2015), object detection (Chen et al., 2018, 2021; Li et al., 2022), and semantic segmentation (Tsai et al., 2018; Zheng and Yang, 2021; Zhang et al., 2021). The application of UDA for semantic segmentation is particularly crucial, as it helps avoid the laborious task of pixel-wise annotation in new target scenarios. Recent UDA approaches for semantic segmentation can be broadly categorized into two paradigms: adversarial training-based methods and self-training-based methods. Adversarial training-based methods focus on learning domain-invariant representations through a min-max adversarial optimization game (Toldo et al., 2020; Tsai et al., 2018). In this paradigm, a feature extractor is trained to confuse a domain discriminator, thereby aligning feature distributions across domains. Self-training-based methods, on the other hand, have gained prominence due to the domain-robustness property of Transformers (Bhojanapalli et al., 2021). These methods generate pseudo labels for target images

based on a teacher-student optimization framework (Tranheden et al., 2021; Hoyer et al., 2022; Luo et al., 2024). The key to the success of this paradigm lies in generating high-quality pseudo labels through strategies such as entropy minimization (Chen et al., 2019), consistency regularization (Hoyer et al., 2023), and class-balanced training (Li et al., 2022). Our approach follows the self-training paradigm and further introduces a general domain bridging mechanism to enhance the performance of existing works. By constructing intermediate domains through a diffusion forward process, we facilitate the gradual transfer of knowledge across different domains and alleviate the semantic shift problem in the intermediate domains.

2.2 Domain Bridging (DB)

Directly transferring knowledge from the source domain to the target domain can be challenging due to significant discrepancies and pixel-wise gaps between the domains. To address this issue, some works propose gradually transferring knowledge by building a bridge between the source and target domains. This is achieved by constructing intermediate domains at the image level (Na et al., 2021; Xu et al., 2020; Yang and Soatto, 2020), feature level (Cui et al., 2020; Dai et al., 2021; Lu et al., 2023), or output level (Huo et al., 2022; Zhang et al., 2021). One line of work utilizes style transfer techniques (Chen et al., 2019; Choi et al., 2019; Gong et al., 2019) to transfer the style of source data to target data, effectively creating intermediate domains. Another approach leverages data mix augmentation techniques (Tranheden et al., 2021; Zhou et al., 2022; Chen et al., 2022), such as CutMix (Yun et al., 2019) and Mixup (Zhang et al., 2017), to construct various intermediate domains. While these methods can effectively reduce the domain gap and facilitate the adapting ability of models, they have certain limitations. Style transfer-based methods are often dataset-specific and may generate unexpected artifacts, while data mix strategies can disrupt the contextual distribution of images and require intricate designs. Both approaches lack generalization ability and face the semantic shift problem, where the intermediate domains may not preserve the semantic information of the original

domains. These limitations restrict their applicability in different scenarios. In contrast, our work aims to explore a universal and concise domain bridging strategy that can be easily integrated into existing UDA frameworks while explicitly compensating for the discriminative representations. By constructing intermediate domains through a diffusion forward process, we propose a dataset-agnostic approach that alleviates the semantic shift problem and enhances the generalization ability of the model.

2.3 Generative Models for Segmentation

Generative models, such as Generative Adversarial Networks (GANs) (Goodfellow et al., 2014) and Variational Autoencoders (VAEs) (Kingma and Welling, 2013), aim to map data points to latent codes that adhere to a straightforward elementary (Gaussian) distribution, enabling the generation and manipulation of data points. Recently, Denoising Diffusion Probabilistic Models (DDPMs) (Ho et al., 2020) have gained attention for their ability to consider the transport mapping problem as a Markov chain and split the process into multiple steps by constructing a series of intermediate distributions between real data and latent codes. To apply these generative mechanisms to semantic segmentation, which is typically a discriminative paradigm, some prior works propose synthesizing images and their corresponding mask labels to train a separate segmentation network (Li et al., 2022; Zhang et al., 2021). Other approaches leverage the internal features extracted by generative models to perform segmentation directly (Xu et al., 2023; Baranchuk et al., 2021). In the context of domain adaptive segmentation, recent diffusion-based methods have shown promising results. One category of work utilizes the generative capability of diffusion models to synthesize diverse domain distributions (Peng et al., 2023; Niemeijer et al., 2024), thereby enhancing the model’s generalization ability. Another line of work considers using the distribution modeling capability of diffusion models to estimate the uncertainty of the segmentation model (Du and Li, 2023), enabling the selection of appropriate training samples for domain adaptation tasks. Unlike these methods, our work incorporates the training strategies of

diffusion models into the self-training framework for domain-adaptive semantic segmentation, facilitating the learning of knowledge from images sampled in arbitrary intermediate distributions. By leveraging the expressive power of diffusion models, our approach aims to bridge the gap between source and target domains more effectively and improve the performance of existing UDA methods.

3 Methods

In this section, we first formalize the standard self-training paradigm for UDA and the training process for diffusion models, respectively (Sec. 3.1). Then, we describe our new UDA framework, DiDA, a universal degradation-based bridging technique that couples diffusion strategies to improve UDA semantic segmentation performance (Sec. 3.2). Finally, we illustrate the details that expand our method to arbitrary choices of image degradation (Sec. 3.3).

3.1 Preliminary Knowledge

3.1.1 Self-Training (ST) for UDA

For domain-adaptive semantic segmentation, the source domain can be denoted as $D_s = \{(x_i^S, y_i^S)\}_{i=1}^{N_s}$, where $x_i^S \in X_S$ represents an image with $y_i^S \in Y_S$ as the corresponding pixel-wise one-hot label covering C classes. The target domain can be denoted as $D_t = \{(x_i^T)\}_{i=1}^{N_t}$, which shares the same label space but has no access to the target label Y^T . In this setting, the supervised loss \mathcal{L}^S can only be calculated on the source domain to train a neural network f_θ :

$$\mathcal{L}^S = \sum_{i=1}^{N_s} \mathcal{L}_{ce}(f_\theta(x_i^S), y_i^S, 1), \quad (1)$$

where \mathcal{L}_{ce} denotes the pixel-wise cross-entropy loss:

$$\mathcal{L}_{ce}(\hat{y}_i, y_i, q_i) = - \sum_{j=1}^{H \times W} \sum_{c=1}^C q_{(i,j,c)} y_{(i,j,c)} \log \hat{y}_{(i,j,c)}. \quad (2)$$

Self-training introduces a teacher-student framework to generate pseudo-labels p^T for the target

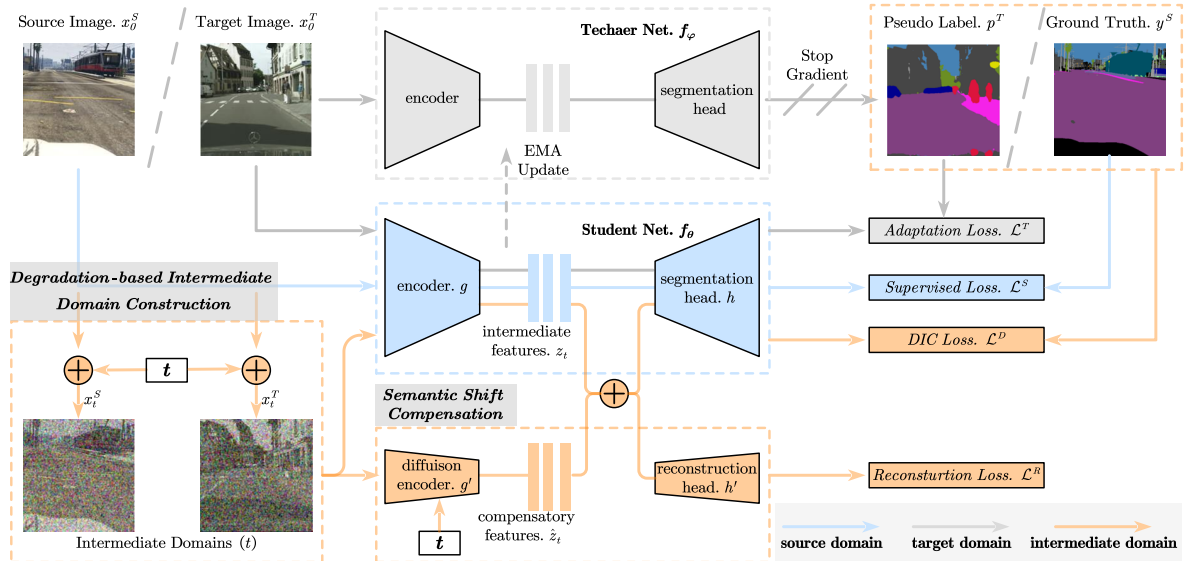


Fig. 2 Overview of the proposed DiDA framework. We integrate diffusion strategies (orange box) with a standard self-training paradigm. While regular frameworks train networks using supervised loss on source domain and unsupervised adaptation loss on target domain, DiDA introduces degradation-based intermediate domains and addresses semantic shift through a diffusion encoder and reconstruction head, which are enabled by degraded image consistency (DIC) loss and reconstruction loss.

domain (see Fig. 2):

$$p_{(i,j,c)}^T = [c = \operatorname{argmax}_{c'} f_\phi(x_i^S)_{(j,c')}], \quad (3)$$

where f_ϕ is the teacher model. Then, the pseudo-labels are used to train the network f_θ on the target domain with the adaptation loss \mathcal{L}^T .

$$\mathcal{L}^T = \sum_{i=1}^{N_T} \mathcal{L}_{ce}(f_\theta(x_i^T), p_i^T, q^T). \quad (4)$$

The quality of pseudo-labels is weighted by a confidence estimate q^T (Hoyer et al., 2022), which gradually strengthens with increasing accuracy of models. After each training step, the teacher model f_ϕ is updated with the exponentially moving average of the weights of f_θ . The segmentation model, f_θ , can be defined as $f_\theta = h \circ g$, where $g: \mathcal{X} \rightarrow \mathcal{Z}$ is an encoder that lifts each pixel of the input image in \mathcal{X} to the feature space \mathcal{Z} , and $h: \mathcal{Z} \rightarrow \mathbb{R}^C$ is a segmentation head which can be viewed as a pixel-wise classifier to give a score for each class.

3.1.2 Diffusion Model

Diffusion models learn a series of state transitions to generate high-quality sample from the noise, defined as a forward diffusion process during the training phase. The diffusion process generates intermediate state x_t with a random uniformly sampled t from $\{1, \dots, T\}$:

$$q(x_t|x_0) = \mathcal{N}(x_t; \sqrt{\bar{\alpha}_t}x_0, (1 - \bar{\alpha}_t)\mathbf{I}), \quad (5)$$

where $\bar{\alpha}_t$ originates from a predefined noise schedule (decreases from 1 to 0). This process can be rewritten through a reparameterization trick:

$$x_t \triangleq \sqrt{\bar{\alpha}_t}x_0 + \sqrt{1 - \bar{\alpha}_t}\epsilon, \quad \epsilon \sim \mathcal{N}(0, \mathbf{I}). \quad (6)$$

Afterward, a network is trained to predict noise ϵ (or predict sample data x_0 directly) from x_t , with a reconstruction loss:

$$\mathcal{L}^R = \|f_\theta(x_t, t) - \epsilon\|_2^2. \quad (7)$$

Algorithm 1 Pseudo algorithms of DiDA.

```
1: Inputs: Source Domain  $D_s = (x_i^S, y_i^S)_{i=1}^{N_s}$ , Target Domain  $D_t = (x_i^T)_{i=1}^{N_T}$ 
2: Define: Student Network  $f_\theta$ , Teacher Network  $f_\phi$ , Diffusion Encoder  $g'$ , Reconstruction Head  $h'$ ,
   Noise Schedule  $\bar{\alpha}_t$ , Diffusion Steps  $T$ , Momentum Coefficient  $\beta$ 
3: Output: Student Network  $f_\theta$ 
4: for each batch of  $(x_i^S, y_i^S), x_i^T$  in  $D_s, D_t$  do
5:   # Source Domain:
6:   Calculate  $\mathcal{L}^S$  for  $f_\theta$  by Eq. (1) ▷ Supervised loss
7:   # Target Domain:
8:   Obtain pseudo-labels from  $f_\phi$  by Eq. (3)
9:   Calculate  $\mathcal{L}^T$  for  $f_\theta$  by Eq. (4) ▷ Adaptation loss
10:  # Degradation-based Intermediate Domain Construction:
11:  Sample  $t \sim \text{Uniform}(1, T)$ 
12:  Obtain degraded images  $x_{i,t}^S, x_{i,t}^T$  by Eq. (6)
13:  # Semantic Shift Compensation:
14:  Calculate  $\mathcal{L}^D$  for  $\hat{f}_\theta = h \circ (g + g')$  by Eq. (10) ▷ Degraded image consistency loss
15:  Calculate  $\mathcal{L}^R$  for  $\hat{f}_\theta = h' \circ (g + g')$  by Eq. (7) ▷ Reconstruction loss
16:  # Training:
17:  Gradient backward  $\mathcal{L}^S + \mathcal{L}^T + \lambda_D \mathcal{L}^D + \lambda_R \mathcal{L}^R$  ▷ Update student model
18:  # EMA Update:
19:   $\phi \leftarrow \beta \phi + (1 - \beta)\theta$  ▷ Update teacher model
20: end for
```

3.2 DiDA Framework

Although intermediate domains facilitate cross-domain adaptation, existing construction methods often require dataset-specific designs and introduce semantic shift by disrupting the original data distribution. To overcome these limitations, we propose DiDA with two key modules: **Degradation-based Intermediate Domain Construction** and **Semantic Shift Compensation**. Our framework processes images at varying degradation levels and addresses semantic shift through a dedicated diffusion encoder and reconstruction head. Designed as a general solution, DiDA seamlessly integrates with existing network architectures and UDA methods.

3.2.1 Degradation-based Intermediate Domain Construction

Our method establishes intermediate domains through generalized image degradation operations. Observing existing domain bridging techniques (Fig. 1), we note their common goal: creating intermediate distributions between source and target domains. We propose a concise, universal

approach by formalizing continuous degradation operations as a diffusing forward process to gradually reduce domain discrepancy.

The learning objective of generative models can be framed as finding a transport map $\mathcal{T} : \mathbb{R}^d \rightarrow \mathbb{R}^d$ between two distributions, i.e., $X = \mathcal{T}(Z)$, where $X \sim \pi_x, Z \sim \pi_z$. Typically, Z follows a simple elementary (Gaussian) distribution for sampling to generate X from the data distribution π_x . In the diffusion process, the transport map is formulated as a Markov chain with learned Gaussian transitions starting at $X_T \sim \pi_z$:

$$X_T \rightarrow X_{T-1} \cdots X_t \xrightarrow{p_\theta(X_{t-1}|X_t)} X_{t-1} \cdots \rightarrow X_0, \quad (8)$$

which is termed as a reverse process in contrast to equation (5). In our case, $X_0 \sim \pi_s, \pi_t$ represents the distribution of the source or target domain, respectively. Since X_1, X_2, \dots, X_T can be viewed as latent codes of the same dimensionality as the data X_0 , we consider them as intermediate domains, which possess gradually decreasing distribution discrepancies compared to the original X_0 . This formulation enables a degradation-based

domain bridging mechanism within the diffusion framework.

3.2.2 Semantic Shift Compensation

While intermediate domains help bridge the distribution gap, they can lead to loss of discriminative representations due to semantic shift. To address this challenge, we propose a compensation mechanism that effectively aligns the extracted features with label semantics throughout the degradation process. Our approach uniquely integrates diffusion strategies with the self-training paradigm by encoding semantic shift information through degradation time-steps, enabling the network to process intermediate domains at any degradation level while maintaining semantic consistency.

In this module, a trainable diffusion encoder, g' , is introduced to map each degraded image x_t to the feature space \hat{Z} given t . This diffusion encoder g' is designed to capture the semantic shift information of the segmentation network’s encoder g when taking x_t as input. To this end, a time embedding module is added to specify the diffusion time t . It is implemented by the Transformer sinusoidal position embedding (Vaswani et al., 2017) to condition all blocks of g' on t . Then, the internal feature $z'_{(t,i)}$ in $block'_i$ is modulated with shift and bias:

$$\hat{z}_{(t,i)} = z'_{(t,i)}(MLP_s^i \circ Embed(t) + 1) + MLP_b^i \circ Embed(t), \quad (9)$$

which is operated at the channel dimension of $z'_{(t,i)}$. The resulting feature \hat{z}_t is required to compensate for the intermediate feature z_t from g to minimize the reconstruction error by being supervised with the loss L^R (see equation (7)), where f_θ is replaced by $\hat{f}_\theta = h' \circ (g + g')$. We perform feature fusion by adding hierarchical features through residual connections. Through this module, the network possesses the power to sense the degree of perturbation precisely and align the extracted features with label semantics by compensating them with semantic shift information. These strategies endow the model with the denoising property to reduce the impact of the decreased ability to learn discriminative representations from degraded images and adapt the knowledge to the original domain distribution.

To leverage intermediate domains for improved adaptation, we introduce a Degraded Image Consistency (DIC) loss:

$$\mathcal{L}^D = \sum_{i=1}^{N_S} \mathcal{L}_{ce}(\bar{f}_\theta(x_{i,t}^S, t), y_i^S, 1) + \sum_{i=1}^{N_T} \mathcal{L}_{ce}(\bar{f}_\theta(x_{i,t}^T, t), p_i^T, q^T), \quad (10)$$

where $\bar{f}_\theta = h \circ (g + g')$ and $x_{i,t}$ is degrade image of $x_{i,0}$, which can be obtained with equation (6). This loss enforces consistency between predictions on degraded and original images.

3.2.3 Training and Inference

The entire training pipeline is shown in Fig. 2 and Alg. 1. The original operation in the self-training framework is fully retained, and our method can be considered as an additional plugin. In each training iteration, we conduct the forward process with a fixed noise schedule $\bar{\alpha}_t$ and random t sampled from a uniform distribution between 1 and T on the current training batch. Then, they are fed to the network $\bar{f}_\theta/\hat{f}_\theta$, which shares the same weights with student net f_θ , and diffusion time t is encoded through the time embedding module in diffusion encoder g' . The outputs of this step, prediction for segmentation map and noise, are individually supervised by DIC loss and reconstruction loss. The overall loss \mathcal{L} for DiDA is the weighted sum of the presented loss components:

$$\mathcal{L} = \mathcal{L}^S + \mathcal{L}^T + \lambda_D \mathcal{L}^D + \lambda_R \mathcal{L}^R. \quad (11)$$

For regular inference, the input is an unprocessed image from X_0 , and there is no need to use the diffusion encoder or reconstruction head for noise prediction, meaning that no additional time consumption or network structure changes are required in this stage.

3.3 Expansion to Arbitrary Degradation

Diffusion models demonstrate flexibility in their choice of degradation operations beyond traditional Gaussian noise (Bansal et al., 2022). Building on this insight, we extend DiDA to support various degradation types while maintaining our

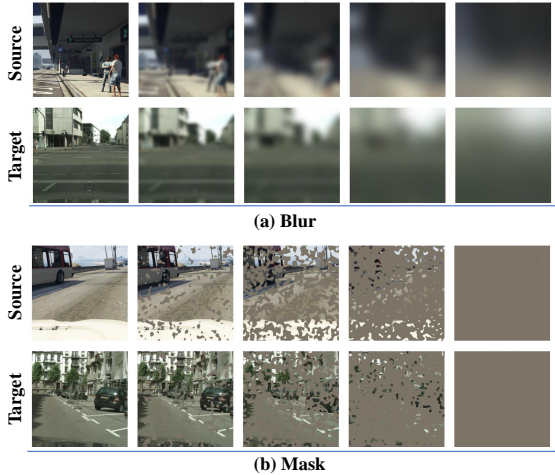


Fig. 3 The examples that extend our method to any other forward diffusion process defined by arbitrary image degradation operations. (a) shows image blurred process and (b) shows image masked process.

core principles of intermediate domain construction and semantic shift perception. To demonstrate this generalization, we implement forward diffusion processes based on two fundamental vision tasks: deblurring and inpainting, as illustrated in Fig. 3. These implementations preserve the network’s ability to perceive degradation levels and compensate for semantic shifts across different degradation operations.

Image Blur. Given the Gaussian kernels $\{G_s\}$, the forward process can be simply defined as:

$$x_t = G_t * x_{t-1} = G_t * \dots * G_1 x_0 = \bar{G}_t * x_0, \quad (12)$$

where $*$ represents the convolution operator to apply the Gaussian blur operation on the image. Then, the model \hat{f}_θ is trained for deblurring to invert this blurred diffusion process.

Image Mask. To implement the incremental mask operation on the image with the diffusion time steps, we define this process with cowmask (French et al., 2020). With the schedule $\bar{\alpha}_t$ as a threshold, we can generate the cowmask \mathcal{M}_t and obtain x_t by element-wise multiplication of the mask and image:

$$x_t = \mathcal{M}_t \odot x_0, \quad (13)$$

and the inpainting model is trained to restore the image.

To extend our method with the above-defined forward process, we only need to replace the degraded image sampling operation and modify the reconstruction loss to predict the clean image x_0 directly:

$$\mathcal{L}^R = \lambda_t \|\hat{f}_\theta(x_t, t) - x_0\|_2^2, \quad (14)$$

where λ_t is a t -dependent loss weight, defined as a fixed value computed from the noise schedule $\{\alpha_t\}_{t=1}^T$ (Salimans and Ho, 2022), introduced to balance the contribution of different degradation levels.

4 Experiments

4.1 Implementation Details

4.1.1 Datasets

To comprehensively evaluate the performance of our proposed method in unsupervised domain adaptation (UDA) tasks, we follow standard UDA protocols and conduct experiments on two widely-used benchmark datasets, transferring knowledge from a synthetic domain to a real domain in a street scene setting. Specifically, we select GTA v (Richter et al., 2016) and SYNTHIA (Ros et al., 2016) as the labeled source domains, while using Cityscapes (Cordts et al., 2016) as the unlabeled target domain. The GTA v dataset contains 24,966 synthetic images with a resolution of 1914×1052 , while the SYNTHIA dataset consists of 9,400 synthetic images with a resolution of 1280×760 . As a real-world urban dataset, Cityscapes comprises 2,975 images for training and 500 images for validation, each with a resolution of 2048×1024 pixels. It is worth noting that previous works adopt different strategies when handling these datasets. For example, (Tsai et al., 2018; Hoyer et al., 2022) downsample Cityscapes to 1024×512 and adjust GTA to 1280×720 . In contrast, HRDA (Hoyer et al., 2022) and MIC (Hoyer et al., 2023) maintain the original resolution of Cityscapes and resize GTA v to 2560×1440 and SYNTHIA to 2560×1520 pixels. In our experiments, we flexibly adopt these different settings based on the characteristics of the methods being built upon.

Table 1 Quantitative results (mIoU in %) of DiDA with different UDA methods, networks, and source domains on Cityscapes val.

Method	GTA. \rightarrow CS.		SYN. \rightarrow CS.	
	C	T	C	T
DAFormer (Hoyer et al., 2022)	56.0	68.3	54.7	60.9
+DiDA	58.3 \uparrow _{2.3}	70.3 \uparrow _{2.0}	57.6 \uparrow _{2.9}	63.1 \uparrow _{2.2}
HRDA (Hoyer et al., 2022)	63.0	73.8	61.2	65.8
+DiDA	64.3 \uparrow _{1.3}	75.4 \uparrow _{1.6}	62.6 \uparrow _{1.4}	67.8 \uparrow _{2.0}
MIC (Hoyer et al., 2023)	64.2	75.9	62.8	67.3
+DiDA	65.0 \uparrow _{0.8}	76.8\uparrow_{0.9}	63.5 \uparrow _{0.7}	68.6\uparrow_{1.3}

4.1.2 Evaluation Metric

To thoroughly assess the performance of our method, we report the intersection over union (IoU) for each class as well as the mean IoU (mIoU) over all classes. Under the GTA $v\rightarrow$ Cityscapes(Val.) setting, we report the IoU results for 19 classes. For the SYNTHIA \rightarrow Cityscapes(Val.) setting, we report the IoU results for 16 classes. These metrics provide a comprehensive reflection of the segmentation performance of our method across different categories.

4.1.3 Base Segmentation Architectures and UDA Methods.

To demonstrate the versatility and adaptability of our method, we implement it on two widely-used network architectures and three progressively enhanced baseline methods. Specifically, we employ DeepLabV2 (Chen et al., 2017) with ResNet-101 (He et al., 2016) backbone and DAFormer (Hoyer et al., 2022) with MiT-B5 (Xie et al., 2021) backbone. Both of these network architectures have been pretrained on the ImageNet-1k (Deng et al., 2009) dataset, exhibiting strong feature extraction and representation capabilities. Building upon this foundation, we apply our framework to different methods in the DAFormer series, including DAFormer (Hoyer et al., 2022), HRDA (Hoyer et al., 2022), and MIC (Hoyer et al., 2023). By conducting experiments on these diverse architectures and methods, we can comprehensively evaluate the effectiveness and robustness of our approach.

4.1.4 Training Details

We implement our method, DiDA, based on the MMSegmentation (Contributors, 2020) framework. Depending on the complexity of the network architectures and UDA frameworks, all experiments are conducted on one or two RTX-3090 GPUs with 24 GB memory, with 40K training iterations and a batch size of 2. We train the network using the AdamW optimizer, with learning rates of 6×10^{-5} for the encoder and 6×10^{-4} for the decoder, a weight decay of 0.01, and a linear learning rate warm-up strategy for the first 1.5K iterations. The input images are scaled and randomly cropped to a size of 512×512 , following the same data augmentation approach as in DAFormer (Hoyer et al., 2022). The exponential moving average (EMA) coefficient for updating the teacher network is set to 0.999. We set the number of diffusion timesteps $T = 100$ and use a sigmoid schedule (Jabri et al., 2022) to obtain $\bar{\alpha}_t$. To achieve scale and quantity matching during feature fusion, we initialize an encoder with the same structure as the corresponding encoder of the segmentation network, along with extra time embedding modules, as the diffusion encoder h' . For the reconstruction head g' , we initialize an ASPP module (Chen et al., 2017) with a linear projector. When computing the reconstruction loss, the clean image x_0 or sampled noise ϵ is down-sampled at a rate of $4\times$ or $8\times$ to match the input of the reconstruction head. We set the weight of the diffusion-induced contrastive (DIC) loss λ^D to 0.5, and the weight of the reconstruction loss λ^R to 5 for DAFormer and 1 for DeepLabV2, ensuring that the gradient magnitudes induced by these different components are comparable. Finally, we calculate the mIoU using the last checkpoint of the student model f_θ without model selection.

Table 2 UDA segmentation performance on GTA. \rightarrow CS, where the highest accuracy in each column is marked as **bold**. The results are acquired based on DeepLabV2 (Chen et al., 2017) with ResNet101 (He et al., 2016) backbone (denoted as C) in the first group and DAFormer (Hoyer et al., 2022) with MiT-B5 (Xie et al., 2021) backbone (denoted as T) in the second group.

Method	Arch.	GTA \rightarrow Citiescapes(Val.)																mIoU			
		Road	Sidewalk	Building	Wall	Fence	Pole	Light	Sign	Veg	Terrain	Sky	Person	Rider	Car	Truck	Bus		Train	Motor	Bike
DACS (Tranheden et al., 2021)	C	89.9	39.7	87.9	39.7	39.5	38.5	46.4	52.8	88.0	44.0	88.8	67.2	35.8	84.5	45.7	50.2	0.2	27.3	34.0	52.1
I2F (Ma et al., 2024)	C	90.8	48.7	85.2	30.6	28.0	33.3	46.4	40.0	85.6	39.1	88.1	61.8	35.0	86.7	46.3	55.6	11.6	44.7	54.3	53.3
ProDA (Zhang et al., 2021)	C	87.8	56.0	79.7	46.3	44.8	45.6	53.5	53.5	88.6	45.2	82.1	70.7	39.2	88.8	45.5	50.4	1.0	48.9	56.4	57.5
DAP (Huo et al., 2024)	C	94.5	63.1	89.1	29.8	47.5	50.4	56.7	58.7	89.5	50.2	87.0	73.6	38.6	91.3	50.2	52.9	0.0	50.2	63.5	59.8
CPSL (Li et al., 2022)	C	92.3	59.5	84.9	45.7	29.7	52.8	61.5	59.5	87.9	41.6	85.0	73.0	35.5	90.4	48.7	73.9	26.3	53.8	53.9	60.8
MIC (Hoyer et al., 2023)	C	96.5	74.3	90.4	47.1	42.8	50.3	61.7	62.3	90.3	49.2	90.7	77.8	53.2	93.0	66.2	68.0	6.8	38.0	60.6	64.2
+DiDA	C	96.6	74.6	89.2	47.5	44.2	50.0	61.2	60.6	90.4	51.9	91.8	76.5	53.8	93.5	67.1	63.7	5.8	50.0	66.7	65.0
TransDA (Chen et al., 2022)	T	94.7	64.2	89.2	48.1	45.8	50.1	60.2	40.8	90.4	50.2	93.7	76.7	47.6	92.5	56.8	60.1	47.6	49.6	55.4	63.9
DAFormer (Hoyer et al., 2022)	T	95.7	70.2	89.4	53.5	48.1	49.6	55.8	59.4	89.9	47.9	92.5	72.2	44.7	92.3	74.5	78.2	65.1	55.9	61.8	68.3
+FST (Du et al., 2022)	T	95.3	67.7	89.3	55.5	47.1	50.1	57.2	58.6	89.9	51.0	92.9	72.7	46.3	92.5	78.0	81.6	74.4	57.7	62.6	69.3
+DiDA (B)	T	97.2	76.3	89.2	58.0	51.1	53.6	57.5	63.5	90.0	51.3	92.3	71.7	43.8	92.1	69.2	81.4	72.1	56.0	64.6	70.0
+DiDA (M)	T	96.4	75.3	90.5	57.6	49.2	53.4	58.6	64.4	90.5	52.6	92.5	71.8	40.8	92.6	70.6	81.7	66.1	57.6	64.0	69.8
+DiDA	T	96.9	74.7	88.9	54.4	49.8	53.5	57.5	63.9	90.6	50.4	92.2	71.5	50.8	92.2	76.1	82.1	70.7	53.2	66.8	70.3
HRDA (Hoyer et al., 2022)	T	96.4	74.4	91.0	61.6	51.5	57.1	63.9	69.3	91.3	48.4	94.2	79.0	52.9	93.9	84.1	85.7	75.9	63.9	67.5	73.8
+DiGA (Shen et al., 2023)	T	97.0	78.6	91.3	60.8	56.7	56.5	64.4	69.9	91.5	50.8	93.7	79.2	55.2	93.7	78.3	86.9	77.8	63.7	65.8	74.3
+DiDA	T	97.4	79.6	91.6	62.9	55.7	59.2	68.0	70.3	92.0	55.5	93.8	80.4	52.5	94.8	86.9	87.0	69.3	66.2	68.9	75.4
MIC (Hoyer et al., 2023)	T	97.4	80.1	91.7	61.2	56.9	59.7	66.0	71.3	91.7	51.4	94.3	79.8	56.1	94.6	85.4	90.3	80.4	64.5	68.5	75.9
+DTS (Huo et al., 2023)	T	97.0	80.4	91.8	60.6	58.7	61.7	7.9	73.2	92.0	45.4	94.3	81.3	58.7	95.0	87.9	90.7	82.2	65.7	69.0	76.5
+DiDA	T	97.9	81.0	92.4	62.0	57.7	60.5	63.2	76.6	92.3	56.4	94.4	79.2	54.4	94.7	86.2	90.4	81.8	65.8	71.6	76.8

Table 3 UDA segmentation performance on SYN. \rightarrow CS., where the highest accuracy in each column is marked as **bold**. The results are acquired based on DeepLabV2 (Chen et al., 2017) with ResNet101 (He et al., 2016) backbone (denoted as C) in the first group and DAFormer (Hoyer et al., 2022) with MIT-B5 (Xie et al., 2021) backbone (denoted as T) in the second group. Note that the mIoUs on are calculated over 16 classes.

Method	Arch.	SYNTHIA \rightarrow Cityscapes(Val.)																			
		Road	Sidewalk	Building	Wall	Fence	Pole	Light	Sign	Veg	Terrain	Sky	Person	Rider	Car	Truck	Bus	Train	Motor	Bike	mIoU
DACS (Tranheden et al., 2021)	C	80.6	25.1	81.9	21.5	2.9	37.2	22.7	24.0	83.7	-	90.8	67.6	38.3	82.9	-	38.9	-	28.5	47.6	48.3
I2F (Ma et al., 2024)	C	84.9	44.7	82.2	9.1	1.9	36.2	42.1	40.2	83.8	-	84.2	68.9	35.3	83.0	-	49.8	-	30.1	52.4	51.8
ProDA (Zhang et al., 2021)	C	87.8	45.7	84.6	37.1	0.6	44.0	54.6	37.0	88.1	-	84.4	74.2	24.3	88.2	-	51.1	-	40.5	45.6	55.5
DAP (Huo et al., 2024)	C	84.2	46.5	82.5	35.1	0.2	46.7	53.6	45.7	89.3	-	87.5	75.7	34.6	91.7	-	73.5	-	49.4	60.5	59.8
CPSL (Li et al., 2022)	C	87.2	43.9	85.5	33.6	0.3	47.7	57.4	37.2	87.8	-	88.5	79.0	32.0	90.6	-	49.4	-	50.8	59.8	57.9
TransDA (Chen et al., 2022)	T	90.4	54.8	86.4	31.1	1.7	53.8	61.1	37.1	90.3	-	93.0	71.2	25.3	92.3	-	66.0	-	44.4	49.8	59.3
DAFormer (Hoyer et al., 2022)	T	84.5	40.7	88.4	41.5	6.5	50.0	55.0	54.6	86.0	-	89.8	73.2	48.2	87.2	-	53.2	-	53.9	61.7	60.9
+FST (Du et al., 2022)	T	88.3	46.1	88.0	41.7	7.3	50.1	53.6	52.5	87.4	-	91.5	73.9	48.1	85.3	-	58.6	-	55.9	63.4	61.9
+DiDA	T	87.8	47.5	88.9	43.1	9.8	51.6	56.8	56.1	86.5	-	90.1	76.1	46.5	88.8	-	56.8	-	59.3	63.2	63.1
HRDA (Hoyer et al., 2022)	T	85.2	47.7	88.8	49.5	4.8	57.2	65.7	60.9	85.3	-	92.9	79.4	52.8	89.0	-	64.7	-	63.9	64.9	65.8
+DiGA (Shen et al., 2023)	T	88.5	49.9	90.1	51.4	6.6	55.3	64.8	62.7	88.2	-	93.5	78.6	51.8	89.5	-	62.2	-	61.0	65.8	66.2
+DiDA	T	87.9	52.9	89.6	54.3	11.6	56.6	63.8	61.2	87.6	-	94.1	79.9	54.2	90.5	-	71.5	-	67.1	62.3	67.8
MIC (Hoyer et al., 2023)	T	86.6	50.5	89.3	47.9	7.8	59.4	66.7	63.4	87.1	-	94.6	81.0	58.9	90.1	-	61.9	-	67.1	64.3	67.3
+DTS (Huo et al., 2023)	T	89.1	54.9	89.0	39.1	8.7	61.6	67.4	64.3	88.8	-	94.0	82.2	60.7	89.6	-	62.6	-	68.5	64.9	67.8
+DiDA	T	89.2	55.9	89.6	49.0	8.4	58.9	66.1	64.4	88.5	-	94.6	80.6	59.4	89.2	-	69.2	-	66.7	68.4	68.6

4.2 Evaluation on Benchmark Datasets

4.2.1 Overall Quantitative Results

Tab. 1 shows the quantitative results and performance comparison by establishing our method upon three recently mainstream methods with different network architectures. We report results based on whole inference on DAFormer and slide inference on HRDA and MIC without any other test time augmentation strategies for a perfectly fair comparison. Whether with Transformer-based (denoted as T) or CNN-based backbones (denoted as C), DiDA achieves consistent gains beyond all three baselines, ranging from 0.7% to 2.9%. As expected, the performance improvement generally decreases when the baseline is stronger and closer to performance saturation. When implemented with DeepLabV2, the performance gain is slightly lower than DAFormer due to the coarse output ($8\times$ downsampling) for the optimization goal of reconstruction. It is worth noting that DiDA achieves new state-of-the-art performance on two benchmarks when applied on MIC, the strongest method before.

4.2.2 Class-level Comparison

We further display the class-wise performance on each benchmark in Tab. 2 and Tab. 3 for detailed comparison. When combined with DiDA, most of the classes achieve higher accuracy. Among these classes, we investigate that performance on *road*, *sidewalk*, *fence*, and *terrain* achieves consistent and relatively significant improvements over all UDA methods and datasets. These classes constitute the main scene and comprise abundant domain-specific texture information. By adding random Gaussian noise to images, these textures are broken while the context information is preserved, which is more robust over domains. Since DiDA establishes domain bridging through these progressively intensifying degraded images between domains, the network can focus more on the context to enhance the adapting ability. Furthermore, we implement the extended version of DiDA on the DAFormer baseline with **Blur** and **Mask**, denoted as **B** and **M**, respectively. These extensions obtain less gain than the default version but show a certain potential if well-designed.

4.2.3 Comparison with other plug-in methods

We further compare DiDA with other plug-in approaches, such as FST (Du et al., 2022), DiGA (Shen et al., 2023), and DTS (Huo et al., 2023). Our method consistently demonstrates superior performance compared to these methods when built with the same baselines.

4.2.4 Qualitative Results

In Fig. 4, we illustrate the qualitative comparisons of our DiDA against DAFormer and MIC. The previous methods fail to identify some classes on the target domain when their visual textures are significantly different from the source domain and confuse them with other visually similar classes (e.g., *sidewalk* and *road*, *fence* and *building*, *terrain* and *vegetation*). In this case, DiDA makes the model recognize semantic categories more dependent on context information, resulting in improved cross-domain performance.

4.3 Diagnostic Experiments

4.3.1 Component Ablation Analysis

To gain deeper insights, we analyze the proposed approach by ablating the components and evaluating the performance with DAFormer as the baseline on GTA→CS. The results are presented in Tab. 4. The DiDA with complete components achieves a 2.0 mIoU gain on this baseline. To analyze the diffusion encoder and the module of time embedding respectively, we use the segmentation encoder g directly conditioned by time embedding as g_{time} without an extra diffusion encoder, as the baseline for ablation studies (row 6). We first ablate the module of time embedding, implying that the original network is equivalently trained with the randomly degraded images as additional data augmentation. The performance decreases heavily in this case (row 2) due to the excessive degradation of data, known as semantic shift problem. The introduced time embedding plays a vital role in encoding noise intensity information, indicating that we alleviate this issue by encoding time-specific semantic shift information. Then, we discard the loss terms, i.e., \mathcal{L}^D and \mathcal{L}^R , respectively (rows 3 and 4). Without \mathcal{L}^R , DiDA obtains less improvement, although it does not

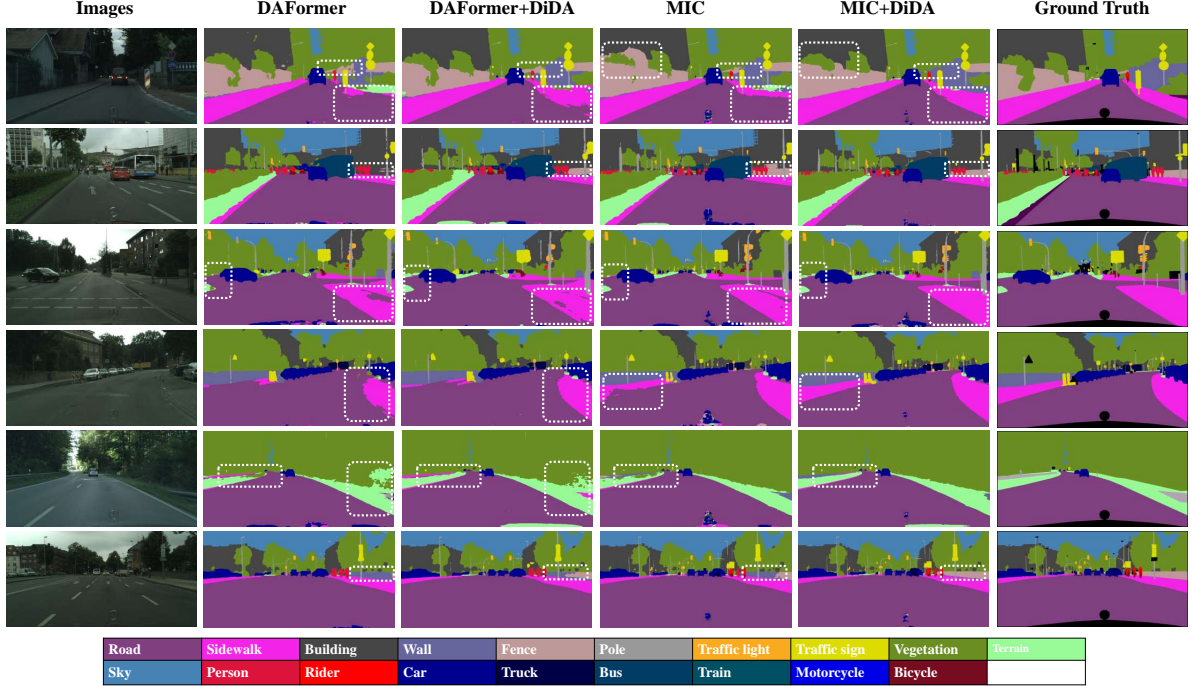


Fig. 4 Qualitative comparison built with DAFormer and MIC. The dotted boxes mark regions improved by DiDA.

Table 4 DiDA ablation study built with DAFormer.

\mathcal{L}^D	\mathcal{L}^R	g_{time}	g'	h'	mIoU
-	-	-	-	-	68.3
✓	-	-	-	-	66.5
✓	-	✓	-	-	69.5
-	✓	✓	-	✓	67.9
✓	✓	✓	-	-	69.4
✓	✓	✓	-	✓	69.9
✓	✓	-	✓	✓	70.3

constrain segmentation results directly, indicating that \mathcal{L}^R helps to learn the module of time embedding and perceive the semantic shift. Discarding \mathcal{L}^D brings an accuracy drop since introducing \mathcal{L}^R only is inconsistent with the learning objective for high-level semantics. After that, the extra reconstruction head h' is ablated (row 5), which means that we obtain reconstruction results from the segmentation head h . It is also essential to avoid excessive disturbance for originally learned features. In the end, the extra diffusion encoder is ablated (rows 6 and 7). Although g_{time} can perceive the semantic shift implicitly enabled by time embedding, it is more effective to introduce an extra diffusion encoder to compensate for the lost discriminative representation.

4.3.2 Influence of Parameter Settings

We further study the influence of parameter settings introduced in DiDA, i.e., DIC loss weight λ_D , reconstruction loss weight λ_R , and diffusion steps T . All experiments are conducted with DAFormer (Hoyer et al., 2022) on GTA→CS.

DIC Loss Weight λ_D . We first study the weight of the DIC loss λ_D in Tab. 5. The weight for the DIC loss is sensitive to the UDA performance. Reducing the weight progressively diminishes performance until no DIC is used. A larger weight also results in decreased performance. If the weight is too large, such as $\lambda_D = 5$, it can lead to a significant decline in performance due to excessive disturbance.

Reconstruction Loss Weight λ_R . The weight of the reconstruction loss is also studied in a similar way (see Tab. 6). Based on the analysis above, we can draw a similar conclusion, with the difference being that this loss item has a slightly diminished impact compared to the previous one. The results demonstrate that values ranging from 1 to 10 consistently yield good UDA performance, providing a reasonably wide range for selecting robust hyperparameters.

Table 5 Parameter study of DIC loss weight λ_D .

Weight λ_D	0	0.1	0.25	0.5	1	5
mIoU	67.9	69.6	70.1	70.3	69.8	64.1

Table 6 Parameter study of reconstruction loss weight λ_R .

Weight λ_R	0	1	2.5	5	10	50
mIoU	69.5	70.0	70.0	70.3	70.2	67.7

Table 7 Parameter study of diffusion steps T .

Diffusion Steps T	10	50	100	200	1000
mIoU	69.3	70.2	70.3	70.0	70.1

Diffusion Steps T . We also study the value selection of diffusion steps T (see Tab. 7). Notice that too large a value, like $T = 1000$, does not result in optimal performance, which is the default setting for DDPM (Ho et al., 2020) to facilitate high-quality generation. In the UDA setting, the number of iterations and batch size is far less than the requirement to train the generative model. Therefore, we make adjustments to reduce the diffusion steps T , ensuring they are more suitable for this task. In our experiments, a value around 100 can achieve consistently good performance.

4.3.3 Influence of Time Schedule

We study different choices of time schedules for β_t , namely, linear (Ho et al., 2020), cosine (Nichol and Dhariwal, 2021), and sigmoid (Jabri et al., 2022), with the same setting as Sec. 4.3.2. The results are summarized in Tab. 8. Although selecting the appropriate schedule is significant for generating high-quality images in the diffusion model, it is robust in DiDA, and we can achieve consistently good performance among these strategies.

4.3.4 More Results with Extended Versions

We further conduct more experiments about **Blur (B)** and **Mask (M)** built with DAFormer (Hoyer et al., 2022) and HRDA (Hoyer et al., 2022) and evaluate the performance on two benchmarks as shown in Tab. 9 and Tab. 10. These extended versions show consistent gains beyond all baselines, which further demonstrates the generality and expansibility of our framework.

Table 8 Different strategies of time schedule.

Time Schedule	linear	cosine	sigmoid
mIoU	69.8	70.2	70.3

Table 9 Results on GTA. \rightarrow CS built with extended versions.

Method	base	B	M
DAFormer (Hoyer et al., 2022)	68.3	70.0	69.8
HRDA (Hoyer et al., 2022)	73.8	75.3	74.9
MIC (Hoyer et al., 2023)	75.9	76.7	76.6

Table 10 Results on SYN. \rightarrow CS built with extended versions.

Method	base	B	M
DAFormer (Hoyer et al., 2022)	60.9	63.1	62.6
HRDA (Hoyer et al., 2022)	65.8	68.0	67.7
MIC (Hoyer et al., 2023)	67.3	68.7	68.2

4.3.5 How DiDA Works

To further comprehend the working mechanism of DiDA, we design two modes for inference on degraded images with known diffusion time t , shown in Fig. 5. The first mode, called implicit denoising inference, is the same as what we used in the training phase of DiDA. The network \bar{f}_θ takes degraded images and t as inputs and generates segmentation results immediately. In contrast with this mode, the second mode segments the degraded images indirectly by predicting the noise through f_θ first for reconstruction and feeding them back to the network \bar{f}_θ , which shares the same weight with \bar{f}_θ but no diffusion encoder, to obtain the final prediction. This mode is termed explicit denoising inference. We evaluate the performance difference between the two modes on different noise levels and construct two performance baselines for comparison. The strong baseline, called base(S), trains and inferences each model separately on intermediate domains with different noise levels. For the weak baseline, termed as base(W), we execute inference on these intermediate domains with f_θ . Fig. 6 (a) plots the performance curve throughout the diffusion forward process. The performance with implicit denoising inference is slightly lower than the explicit mode, and the gap between them is tiny. Both modes beat the strong baseline using a single network trained only once. It indicates that DiDA can perceive the semantic shift precisely and extract

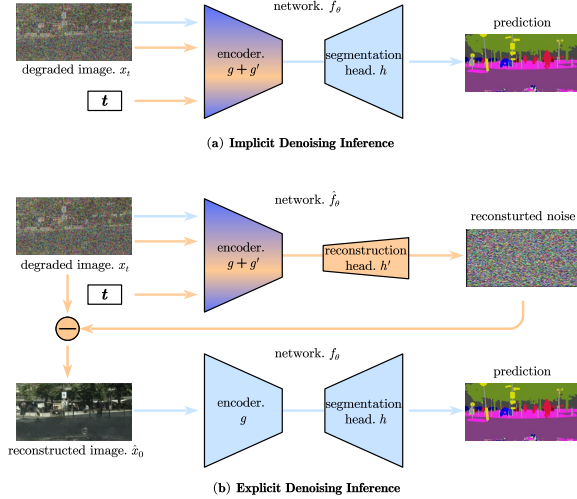
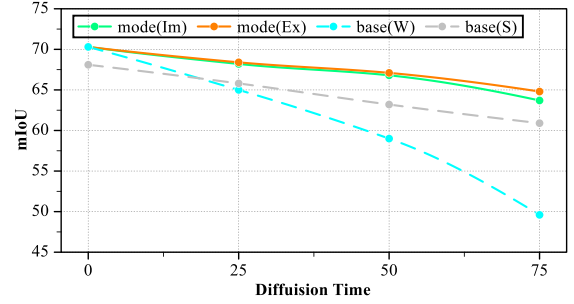


Fig. 5 Demonstration of two modes of inference.

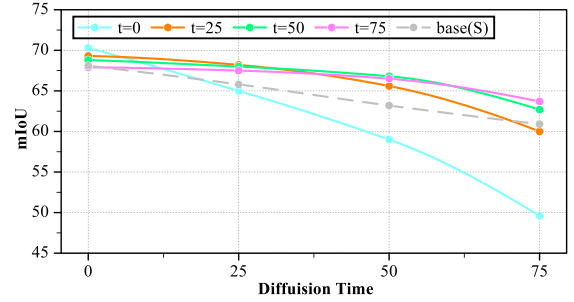
features in an implicit denoising manner during the training procedure, which is how DiDA settles the issue of decreased discriminative representation extraction ability. Furthermore, unlike the explicit mode, the network \bar{f}_θ learns features directly from the degraded images to bridge the domain gap and heighten the adapting ability. These two factors jointly contribute to improving overall performance on UDA segmentation.

4.3.6 Inference with Fixed Diffusion Time

Based on the above discussion, we further evaluate the performance for inference with different fixed diffusion times t . The results are summarized in Fig. 6 (b). Note that $t = 0$ is equivalent to inference without the diffusion encoder, i.e., f_θ , which is the same as the weak baseline defined above. With the change of fixed diffusion time, there are two common properties among these curves: (i) the performance decreases along with the forward diffusion process, and (ii) at each fixed level of the forward process, inference with the same fixed diffusion time t can achieve the current best precision, which is in accordance with the intuition. We can deduce that the higher t is fixed in the inference procedure, the flatter the corresponding performance curve will be. Although the optimal performance degrades, this attribute indicates that we can execute inference with a specific



(a) Ablation for Inference Mode



(b) Ablation for Fixed Time in Inference

Fig. 6 The performance variation with the degraded level.

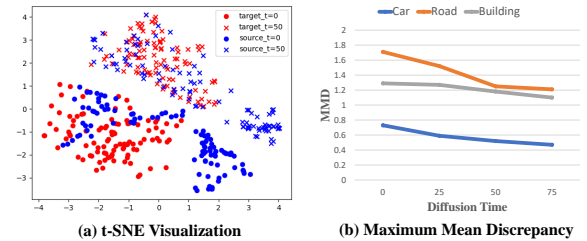


Fig. 7 Comparison of features distribution discrepancy.

value for diffusion time t as input to improve the anti-interference ability of networks.

4.3.7 Degradation-based domain bridging

To further explore the feasibility of our motivation and provide deeper analysis, we show the qualitative and quantitative results to compare the distribution discrepancy between the domains. We train models with $t = 0$ and $t = 50$ separately using DAFormer, then we sample the features of the class "car" in source/target domains and visualize them using t-SNE in Fig. 7 (a). We can see

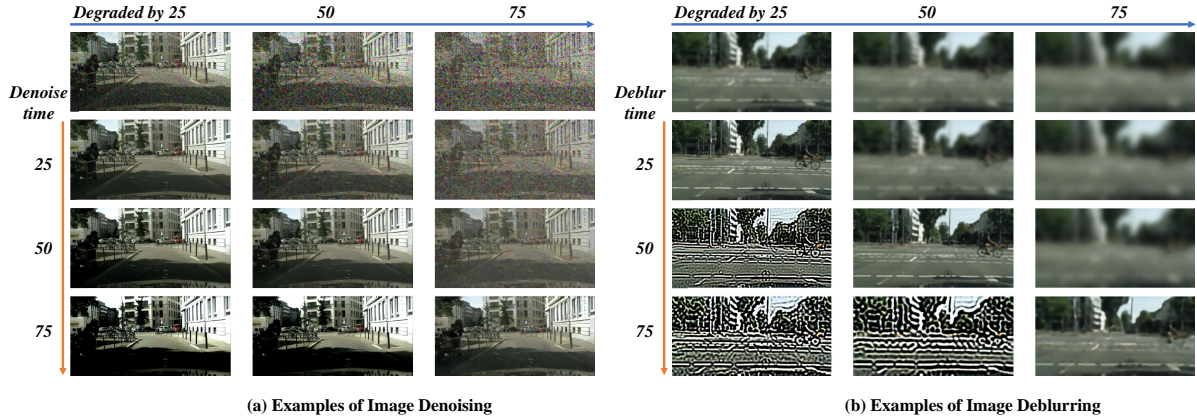


Fig. 8 The examples of image reconstruction results with fixed diffusion time $t = 25, 50, 75$ as input in the time embedding module, where the image is degraded by 25, 50, and 75, respectively.

that the constructed intermediate domains make the feature distribution of source/target data more compact and effectively alleviate the domain gap. We further train models within intermediate domains constructed by different diffusion times, sample the features of the classes "car", "road", and "building", and measure the maximum mean discrepancy (MMD) between source and target domains in Fig. 7 (b). A smaller value of the MMD metric represents a smaller distribution difference. By increasing the level of image degradation, the distribution discrepancy between the two domains gradually decreases, which further confirms our motivation.

4.3.8 Visualization of Reconstruction Results

We visualize examples of reconstruction results in Fig. 8 with $t = 25, 50, 75$ in the time embedding module. The model can yield the best reconstruction results for degraded images with the corresponding t value. A fixed value of t leads to inadequate denoising for higher levels of degradation and excessive denoising for lower levels of degradation, meaning that degradation information is accurately encoded in the time embedding. This further alleviates the semantic shift phenomenon and facilitates adaptive learning from the disturbed image.

5 Conclusions

In this paper, we introduced DiDA, a degradation-based bridging approach for domain adaptive semantic segmentation. Our method constructs intermediate domains through simple image degradation operations and formalizes them as a diffusion forward process, addressing the limitations of existing domain bridging techniques. By integrating image degradation operations into the UDA training pipeline, DiDA encourages the model to learn domain-invariant features and alleviates the semantic shift problem in the intermediate domains. The generality and expansibility of our framework are demonstrated by providing multiple degradation operations, showing that DiDA can be built with any choice of image degradation. Moreover, our plug-and-play bridging technique consistently improves performance when applied to various UDA methods and network architectures. Experimental results on two standard UDA semantic segmentation benchmarks validate the effectiveness of our approach, setting a new state-of-the-art performance.

Declarations

Conflicts of interest. The authors have no financial or proprietary interests in any material discussed in this article.

Data Availability. Cityscapes dataset be downloaded at <https://www.cityscapes-dataset.com/downloads>. GTAv dataset be

downloaded at https://download.visinf.tu-darmstadt.de/data/from_games. SYNTHIA dataset be downloaded at <https://synthia-dataset.net/downloads>.

Code Availability. The codes used in this manuscript will be made publicly available at <https://github.com/Woof6/DiDA>.

Appendix A Details in Expansion Versions

In this section, we describe the details of our implementation for expansion versions of DiDA, in which we replace the degradation operation in the diffusion forward process with **blur** and **mask**.

Image Blur. Following the setting of cold diffusion (Bansal et al., 2022), we define T Gaussian kernels: G_1, \dots, G_T to execute gradual blurring. For instance, we set $T = 100$ with a Gaussian kernel of 31×31 , and the standard deviation of the Gaussian kernel grows exponentially with time t at the rate of 0.02.

Image Mask. We implement it with cowmask (French et al., 2020) and take $\bar{\alpha}_t$ defined before as threshold τ . The procedure for generating a masked image with cowmask and τ is provided in Algorithm 2, and we set the std $\delta = 6$.

Algorithm 2 CowMask generation algorithm with the threshold $\tau \in [0, 1]$ as the ratio in original image.

Require: original image x^O , threshold τ , std δ

Ensure: masked image x^M

- 1: sample Gaussian noise $\epsilon \sim \mathcal{N}(0, \mathbf{I})$
 - 2: filter noise $\epsilon_f = \text{gaussian_filter_2d}(\epsilon, \delta)$
 - 3: compute mean $m = \text{mean}(\epsilon_f)$
 - 4: compute std_dev $s = \text{std_dev}(\epsilon_f)$
 - 5: compute noise threshold $p = m + \sqrt{2} \text{erf}^{-1}(2\tau - 1)s$
 - 6: threshold filtered noise $\mathcal{M} = \epsilon_f < p$
 - 7: mask image $x^M = x^O \odot \mathcal{M}$
 - 8: **return** x^M
-

Appendix B Architecture of Time Embedding Module

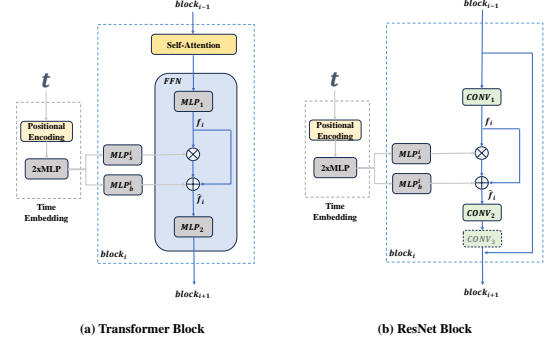


Fig. 9 Architecture of time embedding module in different backbones.

In this section, we illustrate the details of the time embedding module introduced in different backbones. As shown in Fig. 9, we condition all blocks of models on t , whether Transformer-based architecture or CNN-based architecture. The diffusion time t is first encoded by Transformer sinusoidal position embedding (Vaswani et al., 2017) and projected to time embedding through 2 layers MLP. Then, the time embedding is encoded by MLP_s^i and MLP_b^i to obtain shift and bias and ensure the same channel dimension as the corresponding feature. In the end, each block’s internal feature f_i is modulated through multiplication and addition operations at the channel dimension.

Appendix C More Examples for Image Reconstruction

In this section, we give further details, analysis, and examples of image reconstruction. For different versions of the implementation of DiDA, we execute the inference with different diffusion times t on varying levels of image degradation for qualitative analysis.

Image Denoising This is the default setting of DiDA, the noise ϵ' is predicted by network \bar{f}_θ firstly and used to reconstruct the image as:

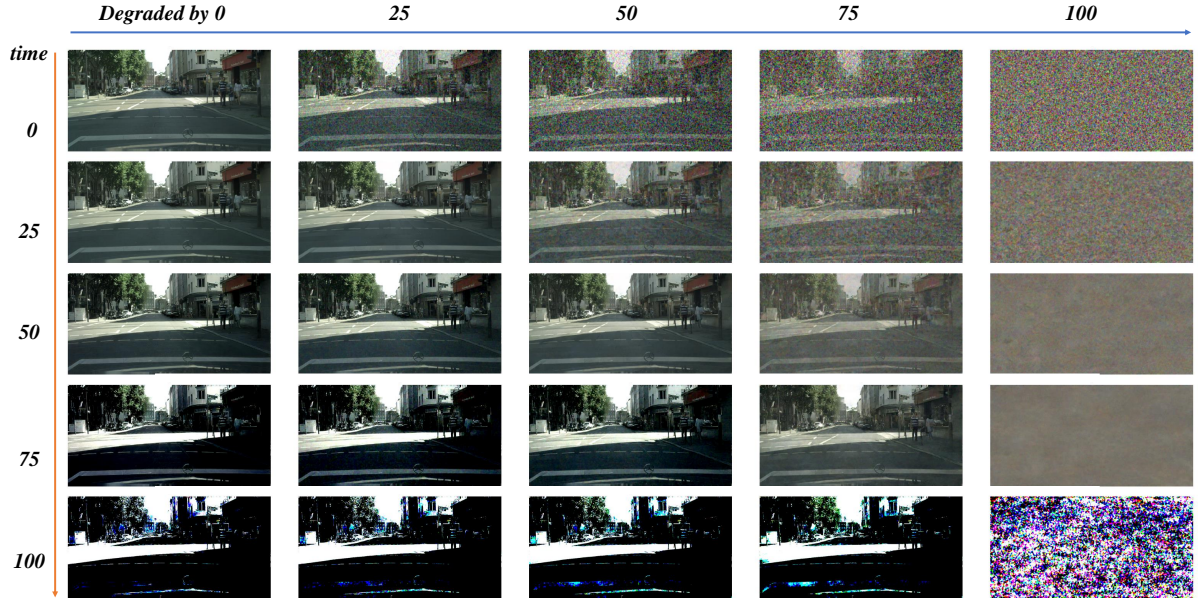


Fig. 10 Examples of image denoising, horizontal coordinate represents the level of image degradation, and vertical coordinate indicates the t used in the inference.

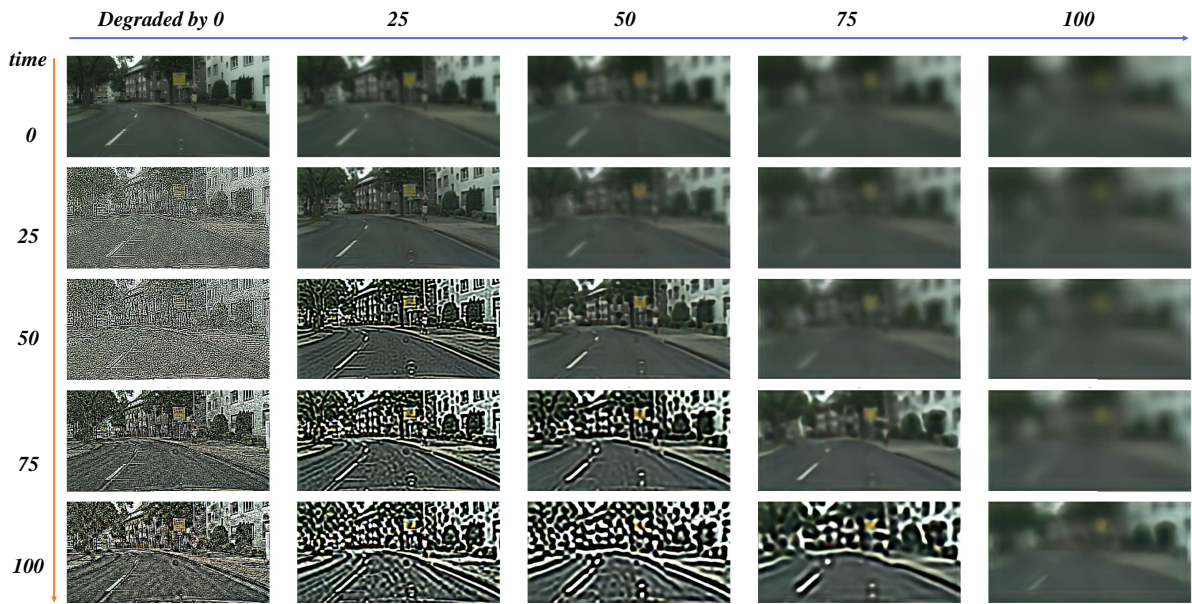


Fig. 11 Examples of image deblurring, horizontal coordinate represents the level of image degradation, and vertical coordinate indicates the t used in the inference.

$$x_0^R = \frac{1}{\sqrt{\alpha_t}}(x_t - \sqrt{1 - \alpha_t}\epsilon_t'). \quad (15)$$

The examples are shown in Fig. 10. The noised images can be restored most perfectly when the diffusion time t matches the level of degradation.

We can observe that the higher value of t has a more powerful anti-noise ability, which is consistent with our experimental results previously stated.

Image Deblurring. In the following two settings, the reconstructed image is directly predicted

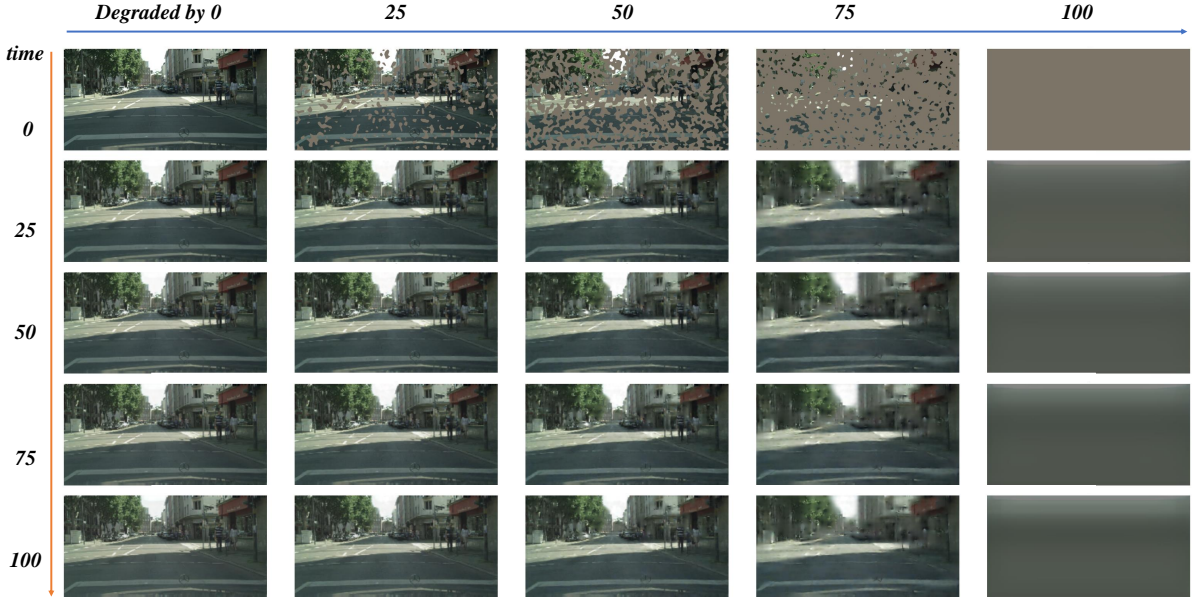


Fig. 12 Examples of image inpainting, horizontal coordinate represents the level of image degradation, and vertical coordinate indicates the t used in the inference.

by \bar{f}_θ . Fig. 11 shows examples of image deblurring. We can draw a similar conclusion that the matched t achieves the best performance as above. The higher t results in excessive deblurring operation while the structure and edge information of the image are preserved, leading to more robust performance.

Image Inpainting. Fig. 12 shows examples of image inpainting. Unlike the former, when the variable t changes in the inference, the reconstruction quality for the masked image does not vary significantly. Since the mask operation is operated in a global view to control the ratio while the previous degrading operation is executed locally, it is difficult for the network to sense the level of degradation in this case. Therefore, DiDA achieves slighter performance gains with the implementation of mask operation.

References

- Long J, Shelhamer E, Darrell T. Fully convolutional networks for semantic segmentation. In: Proceedings of the IEEE conference on computer vision and pattern recognition; 2015. p. 3431–3440.
- Chen LC, Papandreou G, Schroff F, Adam H. Rethinking atrous convolution for semantic segmentation. arXiv preprint arXiv:170605587. 2017;.
- Cheng B, Schwing A, Kirillov A. Per-pixel classification is not all you need for semantic segmentation. Advances in Neural Information Processing Systems. 2021;34:17864–17875.
- Cheng B, Misra I, Schwing AG, Kirillov A, Girdhar R. Masked-attention mask transformer for universal image segmentation. In: Proceedings of the IEEE/CVF conference on computer vision and pattern recognition; 2022. p. 1290–1299.
- Murez Z, Kolouri S, Kriegman D, Ramamoorthi R, Kim K. Image to image translation for domain adaptation. In: Proceedings of the IEEE conference on computer vision and pattern recognition; 2018. p. 4500–4509.
- Hoffman J, Tzeng E, Park T, Zhu JY, Isola P, Saenko K, et al. Cycada: Cycle-consistent adversarial domain adaptation. In: International conference on machine learning. Pmlr; 2018. p. 1989–1998.

- Zhu JY, Park T, Isola P, Efros AA. Unpaired image-to-image translation using cycle-consistent adversarial networks. In: Proceedings of the IEEE international conference on computer vision; 2017. p. 2223–2232.
- Gong R, Li W, Chen Y, Gool LV. Dlow: Domain flow for adaptation and generalization. In: Proceedings of the IEEE/CVF conference on computer vision and pattern recognition; 2019. p. 2477–2486.
- Peng D, Hu P, Ke Q, Liu J. Diffusion-based image translation with label guidance for domain adaptive semantic segmentation. In: Proceedings of the IEEE/CVF International Conference on Computer Vision; 2023. p. 808–820.
- Tranheden W, Olsson V, Pinto J, Svensson L. Dacs: Domain adaptation via cross-domain mixed sampling. In: Proceedings of the IEEE/CVF Winter Conference on Applications of Computer Vision; 2021. p. 1379–1389.
- Olsson V, Tranheden W, Pinto J, Svensson L. Classmix: Segmentation-based data augmentation for semi-supervised learning. In: Proceedings of the IEEE/CVF Winter Conference on Applications of Computer Vision; 2021. p. 1369–1378.
- Zhou Q, Feng Z, Gu Q, Pang J, Cheng G, Lu X, et al. Context-aware mixup for domain adaptive semantic segmentation. *IEEE Transactions on Circuits and Systems for Video Technology*. 2022;33(2):804–817.
- Chen L, Wei Z, Jin X, Chen H, Zheng M, Chen K, et al. Deliberated domain bridging for domain adaptive semantic segmentation. *Advances in Neural Information Processing Systems*. 2022;35:15105–15118.
- Yang Y, Soatto S. Fda: Fourier domain adaptation for semantic segmentation. In: Proceedings of the IEEE/CVF conference on computer vision and pattern recognition; 2020. p. 4085–4095.
- Huo X, Xie L, Zhou W, Li H, Tian Q. Focus on Your Target: A Dual Teacher-Student Framework for Domain-adaptive Semantic Segmentation. *arXiv preprint arXiv:230309083*. 2023;.
- Bai Y, Yang E, Wang Z, Du Y, Han B, Deng C, et al. RSA: reducing semantic shift from aggressive augmentations for self-supervised learning. *Advances in Neural Information Processing Systems*. 2022;35:21128–21141.
- Wang Y, Geng Z, Jiang F, Li C, Wang Y, Yang J, et al. Residual relaxation for multi-view representation learning. *Advances in Neural Information Processing Systems*. 2021;34:12104–12115.
- Ho J, Jain A, Abbeel P. Denoising diffusion probabilistic models. *Advances in neural information processing systems*. 2020;33:6840–6851.
- Ghifary M, Kleijn WB, Zhang M, Balduzzi D, Li W. Deep reconstruction-classification networks for unsupervised domain adaptation. In: *Computer Vision–ECCV 2016: 14th European Conference, Amsterdam, The Netherlands, October 11–14, 2016, Proceedings, Part IV 14*. Springer; 2016. p. 597–613.
- Ganin Y, Ustinova E, Ajakan H, Germain P, Larochelle H, Laviolette F, et al. Domain-adversarial training of neural networks. *Journal of machine learning research*. 2016;17(59):1–35.
- Long M, Cao Y, Wang J, Jordan M. Learning transferable features with deep adaptation networks. In: *International conference on machine learning*. PMLR; 2015. p. 97–105.
- Chen Y, Li W, Sakaridis C, Dai D, Van Gool L. Domain adaptive faster r-cnn for object detection in the wild. In: Proceedings of the IEEE conference on computer vision and pattern recognition; 2018. p. 3339–3348.
- Chen Y, Wang H, Li W, Sakaridis C, Dai D, Van Gool L. Scale-aware domain adaptive faster r-cnn. *International Journal of Computer Vision*. 2021;129(7):2223–2243.
- Li W, Liu X, Yuan Y. Sigma: Semantic-complete graph matching for domain adaptive object detection. In: Proceedings of the IEEE/CVF Conference on Computer Vision and Pattern Recognition; 2022. p. 5291–5300.

- Tsai YH, Hung WC, Schuler S, Sohn K, Yang MH, Chandraker M. Learning to adapt structured output space for semantic segmentation. In: Proceedings of the IEEE conference on computer vision and pattern recognition; 2018. p. 7472–7481.
- Zheng Z, Yang Y. Rectifying pseudo label learning via uncertainty estimation for domain adaptive semantic segmentation. *International Journal of Computer Vision*. 2021;129(4):1106–1120.
- Zhang P, Zhang B, Zhang T, Chen D, Wang Y, Wen F. Prototypical pseudo label denoising and target structure learning for domain adaptive semantic segmentation. In: Proceedings of the IEEE/CVF conference on computer vision and pattern recognition; 2021. p. 12414–12424.
- Toldo M, Michieli U, Agresti G, Zanuttigh P. Unsupervised domain adaptation for mobile semantic segmentation based on cycle consistency and feature alignment. *Image and Vision Computing*. 2020;95:103889.
- Bhojanapalli S, Chakrabarti A, Glasner D, Li D, Unterthiner T, Veit A. Understanding robustness of transformers for image classification. In: Proceedings of the IEEE/CVF international conference on computer vision; 2021. p. 10231–10241.
- Hoyer L, Dai D, Van Gool L. Daformer: Improving network architectures and training strategies for domain-adaptive semantic segmentation. In: Proceedings of the IEEE/CVF Conference on Computer Vision and Pattern Recognition; 2022. p. 9924–9935.
- Luo X, Chen W, Liang Z, Yang L, Wang S, Li C. Crots: Cross-domain teacher–student learning for source-free domain adaptive semantic segmentation. *International Journal of Computer Vision*. 2024;132(1):20–39.
- Chen M, Xue H, Cai D. Domain adaptation for semantic segmentation with maximum squares loss. In: Proceedings of the IEEE/CVF International Conference on Computer Vision; 2019. p. 2090–2099.
- Hoyer L, Dai D, Wang H, Van Gool L. MIC: Masked image consistency for context-enhanced domain adaptation. In: Proceedings of the IEEE/CVF Conference on Computer Vision and Pattern Recognition; 2023. p. 11721–11732.
- Li R, Li S, He C, Zhang Y, Jia X, Zhang L. Class-balanced pixel-level self-labeling for domain adaptive semantic segmentation. In: Proceedings of the IEEE/CVF Conference on Computer Vision and Pattern Recognition; 2022. p. 11593–11603.
- Na J, Jung H, Chang HJ, Hwang W. Fixbi: Bridging domain spaces for unsupervised domain adaptation. In: Proceedings of the IEEE/CVF conference on computer vision and pattern recognition; 2021. p. 1094–1103.
- Xu M, Zhang J, Ni B, Li T, Wang C, Tian Q, et al. Adversarial domain adaptation with domain mixup. In: Proceedings of the AAAI conference on artificial intelligence. vol. 34; 2020. p. 6502–6509.
- Cui S, Wang S, Zhuo J, Su C, Huang Q, Tian Q. Gradually vanishing bridge for adversarial domain adaptation. In: Proceedings of the IEEE/CVF conference on computer vision and pattern recognition; 2020. p. 12455–12464.
- Dai Y, Liu J, Sun Y, Tong Z, Zhang C, Duan LY. Idm: An intermediate domain module for domain adaptive person re-id. In: Proceedings of the IEEE/CVF International Conference on Computer Vision; 2021. p. 11864–11874.
- Lu Z, Li D, Song YZ, Xiang T, Hospedales TM. Uncertainty-aware source-free domain adaptive semantic segmentation. *IEEE Transactions on Image Processing*. 2023;.
- Huo X, Xie L, Hu H, Zhou W, Li H, Tian Q. Domain-agnostic prior for transfer semantic segmentation. In: Proceedings of the IEEE/CVF conference on Computer Vision and Pattern Recognition; 2022. p. 7075–7085.
- Chen YC, Lin YY, Yang MH, Huang JB. Crdoco: Pixel-level domain transfer with cross-domain consistency. In: Proceedings of the IEEE/CVF conference on computer vision and pattern

- recognition; 2019. p. 1791–1800.
- Choi J, Kim T, Kim C. Self-ensembling with gan-based data augmentation for domain adaptation in semantic segmentation. In: Proceedings of the IEEE/CVF International Conference on Computer Vision; 2019. p. 6830–6840.
- Yun S, Han D, Oh SJ, Chun S, Choe J, Yoo Y. Cutmix: Regularization strategy to train strong classifiers with localizable features. In: Proceedings of the IEEE/CVF international conference on computer vision; 2019. p. 6023–6032.
- Zhang H, Cisse M, Dauphin YN, Lopez-Paz D. mixup: Beyond empirical risk minimization. arXiv preprint arXiv:171009412. 2017;.
- Goodfellow I, Pouget-Abadie J, Mirza M, Xu B, Warde-Farley D, Ozair S, et al. Generative adversarial nets. *Advances in neural information processing systems*. 2014;27.
- Kingma DP, Welling M. Auto-encoding variational bayes. arXiv preprint arXiv:1312.6114. 2013;.
- Li D, Ling H, Kim SW, Kreis K, Fidler S, Torralla A. BigDatasetGAN: Synthesizing ImageNet with pixel-wise annotations. In: Proceedings of the IEEE/CVF Conference on Computer Vision and Pattern Recognition; 2022. p. 21330–21340.
- Zhang Y, Ling H, Gao J, Yin K, Lafleche JF, Barriuso A, et al. Datasetgan: Efficient labeled data factory with minimal human effort. In: Proceedings of the IEEE/CVF Conference on Computer Vision and Pattern Recognition; 2021. p. 10145–10155.
- Xu J, Liu S, Vahdat A, Byeon W, Wang X, De Mello S. Open-vocabulary panoptic segmentation with text-to-image diffusion models. In: Proceedings of the IEEE/CVF Conference on Computer Vision and Pattern Recognition; 2023. p. 2955–2966.
- Baranchuk D, Rubachev I, Voynov A, Khruklov V, Babenko A. Label-efficient semantic segmentation with diffusion models. arXiv preprint arXiv:211203126. 2021;.
- Niemeijer J, Schwonberg M, Termöhlen JA, Schmidt NM, Fingscheidt T. Generalization by adaptation: Diffusion-based domain extension for domain-generalized semantic segmentation. In: Proceedings of the IEEE/CVF Winter Conference on Applications of Computer Vision; 2024. p. 2830–2840.
- Du Z, Li J. Diffusion-based probabilistic uncertainty estimation for active domain adaptation. *Advances in Neural Information Processing Systems*. 2023;36:17129–17155.
- Vaswani A, Shazeer N, Parmar N, Uszkoreit J, Jones L, Gomez AN, et al. Attention is all you need. *Advances in neural information processing systems*. 2017;30.
- Bansal A, Borgnia E, Chu HM, Li JS, Kazemi H, Huang F, et al. Cold diffusion: Inverting arbitrary image transforms without noise. arXiv preprint arXiv:220809392. 2022;.
- French G, Oliver A, Salimans T. Milking cowmask for semi-supervised image classification. arXiv preprint arXiv:200312022. 2020;.
- Salimans T, Ho J. Progressive distillation for fast sampling of diffusion models. arXiv preprint arXiv:220200512. 2022;.
- Hoyer L, Dai D, Van Gool L. HRDA: Context-aware high-resolution domain-adaptive semantic segmentation. In: European Conference on Computer Vision. Springer; 2022. p. 372–391.
- Richter SR, Vineet V, Roth S, Koltun V. Playing for data: Ground truth from computer games. In: Computer Vision—ECCV 2016: 14th European Conference, Amsterdam, The Netherlands, October 11–14, 2016, Proceedings, Part II 14. Springer; 2016. p. 102–118.
- Ros G, Sellart L, Materzynska J, Vazquez D, Lopez AM. The synthia dataset: A large collection of synthetic images for semantic segmentation of urban scenes. In: Proceedings of the IEEE conference on computer vision and pattern recognition; 2016. p. 3234–3243.
- Cordts M, Omran M, Ramos S, Rehfeld T, Enzweiler M, Benenson R, et al. The cityscapes

- dataset for semantic urban scene understanding. In: Proceedings of the IEEE conference on computer vision and pattern recognition; 2016. p. 3213–3223.
- Chen LC, Papandreou G, Kokkinos I, Murphy K, Yuille AL. Deeplab: Semantic image segmentation with deep convolutional nets, atrous convolution, and fully connected crfs. *IEEE transactions on pattern analysis and machine intelligence*. 2017;40(4):834–848.
- He K, Zhang X, Ren S, Sun J. Deep residual learning for image recognition. In: Proceedings of the IEEE conference on computer vision and pattern recognition; 2016. p. 770–778.
- Xie E, Wang W, Yu Z, Anandkumar A, Alvarez JM, Luo P. SegFormer: Simple and efficient design for semantic segmentation with transformers. *Advances in Neural Information Processing Systems*. 2021;34:12077–12090.
- Ma H, Lin X, Yu Y. I2F: A Unified Image-to-Feature Approach for Domain Adaptive Semantic Segmentation. *IEEE Transactions on Pattern Analysis and Machine Intelligence*. 2024;46(3):1695–1710.
- Huo X, Xie L, Hu H, Zhou W, Li H, Tian Q. Domain-Agnostic Priors for Semantic Segmentation Under Unsupervised Domain Adaptation and Domain Generalization. *International Journal of Computer Vision*. 2024;p. 1–23.
- Chen R, Rong Y, Guo S, Han J, Sun F, Xu T, et al. Smoothing matters: Momentum transformer for domain adaptive semantic segmentation. *arXiv preprint arXiv:220307988*. 2022;.
- Du Y, Shen Y, Wang H, Fei J, Li W, Wu L, et al. Learning from future: A novel self-training framework for semantic segmentation. *Advances in Neural Information Processing Systems*. 2022;35:4749–4761.
- Shen F, Gurram A, Liu Z, Wang H, Knoll A. DiGA: Distil to Generalize and then Adapt for Domain Adaptive Semantic Segmentation. In: Proceedings of the IEEE/CVF Conference on Computer Vision and Pattern Recognition; 2023. p. 15866–15877.
- Deng J, Dong W, Socher R, Li LJ, Li K, Fei-Fei L. Imagenet: A large-scale hierarchical image database. In: 2009 IEEE conference on computer vision and pattern recognition. Ieee; 2009. p. 248–255.
- Contributors M.: MMSegmentation: Openmmlab semantic segmentation toolbox and benchmark.
- Jabri A, Fleet D, Chen T. Scalable adaptive computation for iterative generation. *arXiv preprint arXiv:221211972*. 2022;.
- Nichol AQ, Dhariwal P. Improved denoising diffusion probabilistic models. In: International Conference on Machine Learning. PMLR; 2021. p. 8162–8171.